International Journal of High Speed Electronics and Systems
Vol. 20, No. 1 (2011) 27–42

DOI: 10.1142/S0129156411006374

World Scientific
www.worldscientific.com

SILICON FINFETS AS DETECTORS OF TERAHERTZ AND SUB-TERAHERTZ RADIATION

W. STILLMAN

Department of Electrical, Computer and Systems Engineering,
Rensselaer Polytechnic Institute, Troy NY 12180, USA
stillw2@rpi.edu

C. DONAIS, S. RUMYANTSEV and M. SHUR

Rensselaer Polytechnic Institute, Troy NY 12180, USA

D. VEKSLER, C. HOBBS, C. SMITH, G. BERSUKER, W. TAYLOR and R. JAMMY

SEMATECH, Austin, TX and Albany, NY, USA

We report on terahertz detection (from 0.2 THz to 2.4 THz) by Si FinFETs of different widths (with 2, 20, and 200 fins connected in parallel). FinFETs (with a small number of fins and with feature sizes as short as 20 nm to 40 nm) showed a very high responsivity (far above that previously measured for standard CMOS). We explain this improvement by negligible narrow channel effects.

Keywords: Terahertz; Detectors; Sensors; Plasma Wave Electronics.

1. Introduction

Within the past several years, the terahertz range of the electromagnetic spectrum has gained ever increasing attention as potential applications emerge in communications, materials identification and imaging [1]. The limited power of available terahertz sources significantly impacts detector performance requirements. In addition, many applications require compact size, fast response time and room temperature operation. Commercially available detectors include pyro-electric devices, Golay cells and Schottky diodes. Typical figures of merit for these devices are summarized in Table 1.

Emerging plasma wave THz and sub-THz detectors have an advantage in their extremely fast speed and are suitable for integration with conventional VLSI technologies. However, their application has been hampered by relatively low responsivity and high Noise Equivalent Power (NEP). Their responsivity varies in a very wide range (from 1 V/W to 1000 V/W depending upon materials system and device structure) and is especially affected by coupling of the THz radiation to the device. In devices without antenna structures, such coupling often involves the contact pads (including the gate pad) and bonding wires [2].

In our present research, we show that since coupling typically involves the gate bonding pad, the device responsivity is decreased by distributive effects of the induced THz current along the gate. Due to this effect only a section of the device close to the bonding pad participates in the THz detection, with the remaining device width effectively shunting the load and decreasing the response. The width of the active section at high frequencies is inversely proportional to the square root of frequency and at high frequencies (above one THz) might be as small as a fraction of a micron. At such small widths however, narrow channel effects might become detrimental to the performance of conventional devices. The FinFET geometry avoids these effects facilitating significant improvements in both responsivity and NEP. In agreement with our model, the decrease in responsivity with frequency of incident radiation becomes less pronounced as the number of device fins decreases.

Table 1 - Commercially Available Room Temperature THz Detectors

	NEP $W/Hz^{1/2}$	Responsivity V/W	Response Time (seconds)	Operating Temp (K)
Golay cells [3]	10^{-10}	10^{5}	10^{-2}	300
Pyroelectrics [4]	10^{-10}	10^{5}	10^{-2}	240-350
Schottky diodes [5]	10^{-12}	10^{3}	10^{-12}	10-420

2. Plasma Wave Detectors

In their seminal paper of 1993, Dyakonov and Shur proposed device operation based on electron plasma waves, localized time-varying perturbations in electron density within the FET channel [6]. This two dimensional electron gas was shown to obey the equations of hydrodynamic motion and continuity, and in their subsequent work on this topic [7, 8] they presented plasma wave devices functioning as detectors and emitters of terahertz radiation and as mixers and frequency multipliers in the terahertz range.

Dependent upon the incident radiation frequency, material momentum relaxation time and device dimension, both resonant and non-resonant detectors were considered. Resonant detection requires the criteria $\omega\tau >> 1$ and $s\tau / L >> 1$, where ω and τ are the angular frequency of the incident radiation and the momentum relaxation time respectively, s is the plasma wave velocity and L is the device channel length. The plasma wave velocity is shown to be dependent upon the gate bias as $s = (q\, V_{gt} /m)^{1/2}$, where q is the electronic charge, m is the electron effective mass and $V_{gt} = V_{gs} - V_t$ is the gate bias swing relative to the threshold voltage V_t. Thus such resonant detectors are tunable via the gate bias. For devices in which $\omega\tau >> 1$ but $s\tau /L << 1$, i.e. relatively longer gates or where $\omega\tau << 1$, i.e. rapid momentum relaxation, detection will be non-resonant, (broadband).

Terahertz detection in silicon devices is typically non-resonant, (although at gate lengths sufficiently short so as to result in ballistic carrier transport, resonant detection in silicon may be possible). The non-resonant DC THz response voltage, δv, of an ideal FET is given by [6]:

$$\delta v = \frac{q v_a^2}{4ms^2}\left\{\frac{1}{1+K\exp\left(-\frac{qV_{gt}}{\eta k_B T}\right)} - \frac{1}{\left[1+K\exp\left(-\frac{qV_{gt}}{\eta k_B T}\right)\right]^2\left(\sinh^2\kappa+\cos^2\kappa\right)}\right\} \quad (1)$$

where v_a is magnitude of the AC voltage induced between the gate and source terminals by the incident radiation and $\kappa = (L/s)(\omega/2\tau)^{1/2}$. Here, η is the device sub-threshold ideality factor, k_B is the Boltzmann constant and T is the temperature in degrees Kelvin. The parameter K (ref. [9] uses κ) resulting in response attenuation in the sub-threshold region is attributed to gate-to-channel leakage current and is calculated from the leakage current density j_0 as:

$$K = \frac{j_0 L^2 m q}{2C\tau\left(\eta k_B T\right)^2} \quad (2)$$

where C is the gate capacitance per unit area. The plasma wave velocity s is calculated from the surface carrier concentration n_s as:

$$s = \left(\frac{q}{m}\frac{n_s}{dn_s/dv}\right)^{1/2} \quad (3)$$

with:

$$n_s = n^* \ln\left[1+\exp\left(\frac{qV_{gt}}{\eta k_B T}\right)\right] \quad (4)$$

where $n^* = C\eta k_B T/q^2$. Thus in the regions above and below the device threshold, $n = CV_{gt}/q$ and $n = n^* exp(qV_{gt}/\eta k_B T)$ respectively, and is interpolated in the region near the threshold.

In contemporary silicon MOSFETs, despite gate dielectric thicknesses on the order of only a few nanometers, gate leakage is often vanishingly small, therefore $K \rightarrow 0$. In the absence of gate leakage, Stillman, et al. [10] attribute response attenuation in the sub-threshold region to voltage division between the device channel resistance and the resistance of the load. With this in mind, eq. (1) may be rewritten as:

$$\delta v = \frac{v_a^2}{4ms^2}\left(\frac{\sinh^2\kappa-\sin^2\kappa}{\sinh^2\kappa+\cos^2\kappa}\right)\left(\frac{1}{1+R_{CH}/R_L}\right) \quad (5)$$

where R_{CH} and R_L are the channel and load resistances, respectively.

Until this point, we have considered only the case where drain current is nearly zero, i.e. "open drain" detection. Lu and Shur first demonstrated the substantial increase in detector response with the application of drain bias [11]. Veksler et al. [12], expand upon this, calculating the response for short samples where $L << s/(\omega/\tau)^{1/2}$ as:

$$\delta v = -\frac{\lambda}{(1-\lambda)^{3/2}} \frac{v_a^2}{4V_{gt}} \tag{6}$$

For long samples where $L >> s/(\omega/\tau)^{1/2}$, the response is given as:

$$\delta v = \frac{v_a^2}{4V_{gt}} \frac{1}{\sqrt{1-\lambda}} \tag{7}$$

In both eqs. (6) and (7), $\lambda = j_d/j_{dsat}$ thus the response rises dramatically as the device is biased into saturation. (While these equations apply only above the device threshold, the more general case which applies to the sub-threshold region was also considered in [12]). While eqs. (5) - (7) accurately predict the response dependence on gate and drain bias, particularly near and below the device threshold and in the region at the onset of saturation, the responsivity of the device is strongly affected by coupling of the THz radiation to the device.

3. FinFET Structure

Dual gate Si MOSFETs were proposed in the early 1990s as a solution to the intractable problem of threshold voltage control as device gate lengths entered the sub-100 nm regime [13-15]. The conventional method of limiting short channel effects by channel doping required untenably high impurity concentrations (on the order of 10^{18} cm^{-3}) likely to degrade device performance through reductions in carrier field mobility and threshold voltage shifts due to quantization of carrier energies [16]. Initial schemes relied on a "vertical" architecture where back and front side gates were placed below and above the device channel. This approach represented significant challenges to existing semiconductor processing. Hisamoto et al. presented an alternative quasi-planar structure in 2000 where the gate conductor wraps around a vertically formed channel "fin"; constructed devices were found to exhibit avoidance of short channel effects with gate lengths as short as 17 nm [17]. The FinFET devices used in our experiments are of similar design, shown schematically in Figure 1, with 2, 20 or 200 fins of 40 nm height and designed widths from 40 to 100 nm. The designed gate length range was from 40 to 100 nm. Fin widths are typically reduced in processing on the order of 10 – 20 nm; gate lengths are expected to be approximately 5 nm shorter than as designed.

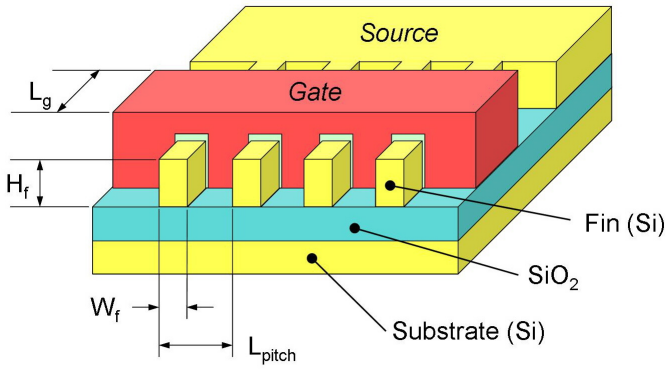

Figure 1 – Schematic illustration of FinFET device structure (the drain region is omitted from the foreground for clarity). The vertical channel fins are surrounded by the gate dielectric and gate conductor forming an effective dual gate MOSFET. Note that the dielectric along the top surfaces of the fin may be increased in order to reduce parasitic capacitance.

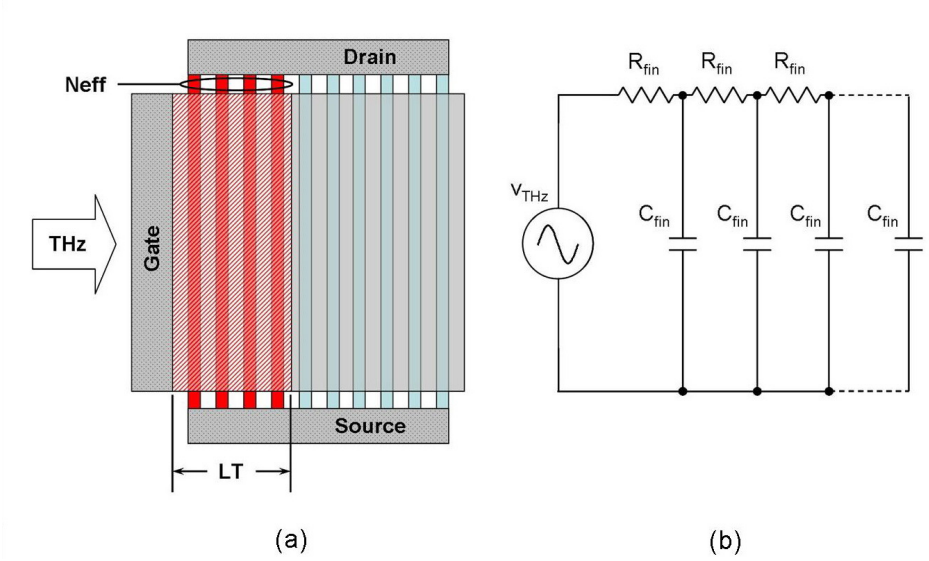

Figure 2 – (a) Conceptual illustration of the effective number of fins (in red) in a given device contributing to response. Fins beyond the characteristic transfer length L_T behave as a load to the response. (b) Schematic representation of equivalent circuit at Terahertz frequencies.

In order to model the frequency dependence of the active area of the FinFET structure we conceptualize the device as shown in Figure 2(a). Here the incident radiation is coupled into the device from the bond pad connection and the signal propagation along the nearly lossless gate conductor transmission line across the device. Figure 2(b) shows the equivalent circuit at THz frequencies. The inductance of the gate conductor is assumed to be greatly overshadowed by that of the bond wires leading to the device and is therefore neglected. Similarly, the conductance of the gate dielectric is neglected since gate leakage is vanishingly small. The fin capacitance, C_{FIN}, and fin access resistance, R_{FIN}, are calculated as:

$$C_{FIN} = \frac{\varepsilon\left(2H_f + W_f\right)L_g}{d} \tag{8}$$

and:

$$R_{FIN} = \frac{\rho_g L_{PITCH}}{L_g} \tag{9}$$

where ε and d are the gate dielectric permittivity and thickness, respectively, L_g is the gate length, H_f and W_f are the fin height and width respectively, L_{PITCH} is the fin pitch and ρ_g is the resistivity of the gate conductor. At some multiple of the characteristic transfer length, L_T, the signal is attenuated so as to be negligible. Only the fins prior to this point, N_{eff}, are effective in contributing to the device response; the remaining fins serve only as an additional load. For a large number of fins, the voltage and current distributions at THz frequency along the gate can be using the telegrapher's equations:

$$\frac{\partial^2 V(x)}{\partial x^2} = \Gamma^2 V(x) \tag{10}$$

and:

$$\frac{\partial^2 I(x)}{\partial x^2} = \Gamma^2 I(x) \tag{11}$$

where $V(x)$ and $I(x)$ are the voltage and current signals along the line respectively, and:

$$\Gamma = \sqrt{j\omega RC} \tag{12}$$

Here ω is the angular frequency of the incident radiation and R and C are the per unit length values of the effective resistance of the gate conductor and the gate capacitance, respectively, calculated as:

$$R = R_{FIN} / L_{PITCH} \tag{13}$$

and:

$$C = C_{FIN} / L_{PITCH} \tag{14}$$

The characteristic impedance of the transmission line is then:

$$Z_0 = \sqrt{\frac{R}{j\omega C}} \tag{15}$$

In the case of reasonably small R, the signal is found to decay as:

$$V(x) = \mathrm{e}^{-x/L_T} \tag{16}$$

with L_T as given by:

$$\left|L_T\right| = \frac{2Z_0}{R} = \frac{2}{\sqrt{\omega RC}} \tag{17}$$

To calculate N_{eff}, L_T is normalized to the fin pitch L_{PITCH} (see Figure 1). While the incident signal is attenuated exponentially along the transmission length, for simplicity we consider only those fins at a distance closer to the gate pad than L_T as contributing to the response and those beyond as passive loads, thus N_{eff} is given by:

$$N_{eff} = \min\left(N, N_{LT}\right) \tag{18}$$

where:

$$N_{LT} = \frac{L_T}{L_{PITCH}} \tag{19}$$

With this expression for N_{eff}, we may calculate the active portion of the multi-channel FET channel resistance (R_A) as:

$$R_A = \frac{1}{N_{eff}}\left[R_S + R_D + \frac{L_g}{\left(2H_f + W_f\right)q\mu n_s}\right] \tag{20}$$

When $N \le N_{eff}$, all device fins are active; when $N > N_{eff}$, the resistance of the passive fins is found as:

$$R_P = \frac{1}{\left(N - N_{eff}\right)}\left[R_S + R_D + \frac{L_g}{\left(2H_f + W_f\right)q\mu n_s}\right] \tag{21}$$

We now consider the effective circuit for the DC THz response as shown in Figure 3(a), and the Thevenin equivalent circuit in Figure 3(b), where:

$$V_{Th} = \delta v \left(\frac{R_P}{R_P + R_A} \right) \tag{22}$$

and:

$$R_{Th} = \frac{R_A R_P}{R_A + R_P} \tag{23}$$

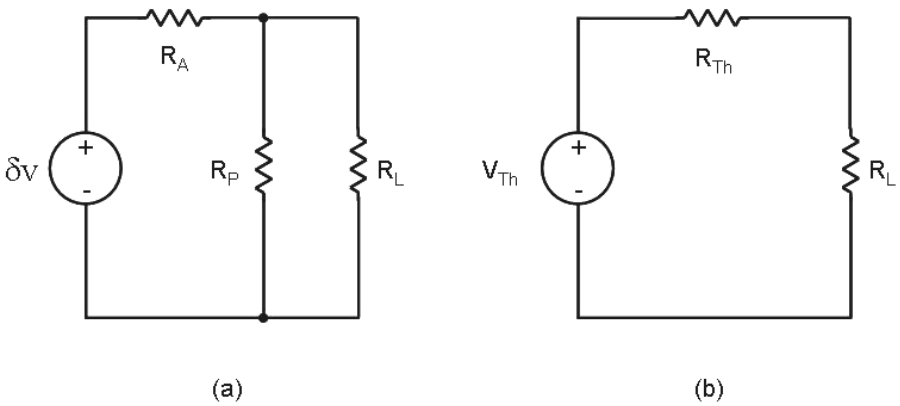

Figure 3 – (a) DC equivalent circuit for FinFET, and (b) Thevenin equivalent representation.

Hence, the detector response is now given by:

$$\delta v_{eff} = \frac{v_a^2}{4ms^2} \left(\frac{\sinh^2 \kappa - \sin^2 \kappa}{\sinh^2 \kappa + \cos^2 \kappa} \right) \frac{R_P R_L}{R_L \left(R_A + R_P \right) + R_P R_A} \tag{24}$$

Until this point, we have ignored the effects of coupling of the incident radiation to the device. While there certainly are a great many factors to consider, for our purpose of modeling the frequency response of the device without an optimized antenna, we consider only the additional effects of the bond wire inductance on the response. We model the attenuation of the incident signal using a lumped parameter voltage divider between the device capacitance and series connected device resistance and bond wire inductance, resulting in the following expression for the effective coupled radiation:

$$v_a = v_{THz} \frac{Z_o}{Z_o + Z_{THz}} \tag{25}$$

Where Z_o is given by eq. (15). We assume that the impedance of the effective THz source is inductive with the effective inductive impedance given by:

$$Z_{THz} = j\omega L_{THz} \tag{26}$$

Combining eqs. (24) and (25) our response expression becomes:

$$\delta v_{eff} = \frac{v_{THz}^2}{4ms^2}\left(\frac{\sinh^2\kappa - \sin^2\kappa}{\sinh^2\kappa + \cos^2\kappa}\right)\left(\frac{R_P R_L}{R_L\left(R_A + R_P\right) + R_P R_A}\right)\left(\frac{Z_o}{Z_o + Z_{THz}}\right)^2 \tag{27}$$

It is expected that this expression will be applicable to the drain current enhanced response of eqs. (6) and (7) with the appropriate adjustments as discussed previously.

The speed of detector response is also of importance. Kachorovskii and Shur [18] propose theoretical calculations of the maximum response modulation frequency in plasma wave detectors as shown in the following expressions:

$$f_{\max} = \begin{cases} \dfrac{\mu_f V_{gt}}{2\pi L_g^2} & V_{gt} > 0, \;\; qV_{gt} >> T \\ \\ \dfrac{\mu_f \eta k_B T}{2\pi q L_g^2} & V_{gt} < 0, \;\; q\left|V_{gt}\right| >> T \end{cases} \tag{28}$$

Here μ_f is the effective field effect mobility, which is very different from conventional mobility for short channel devices, where ballistic or near ballistic transport is dominant. Near $V_{gt} = 0, f_{max}$ is interpolated as:

$$f_{\max} = \left(\frac{\mu_f \eta k_B T}{2\pi q L_g^2}\right)\left[1 + \exp\left(\frac{-qV_{gt}}{\eta k_B T}\right)\right]\ln\left[1 + \exp\left(\frac{qV_{gt}}{\eta k_B T}\right)\right] \tag{29}$$

4. Response Measurements

Prior to response measurements, current / voltage characteristics were performed and die containing several functional devices were wire bonded within ceramic chip carriers to simplify handling. Response measurements were made using a standard lock-in technique. Two radiation source types were used: a purpose built Gunn diode oscillator equipped with frequency multipliers was used at the 0.2 and 0.6 THz. An optically pumped terahertz gas laser was used at 1.6 and 2.4 THz. Source power was measured as 1.5 mW, 35 μW, 30 mW and 10 mW for 0.2, 0.6, 1.6 and 2.4 THz respectively. A chopper was placed in the beam path and the radiation was focused onto the device using either a parabolic mirror or polyethylene lens depending upon the source. Two programmable power supplies were used to provide gate and drain bias. Figure 4 illustrates the typical response dependence upon gate bias.

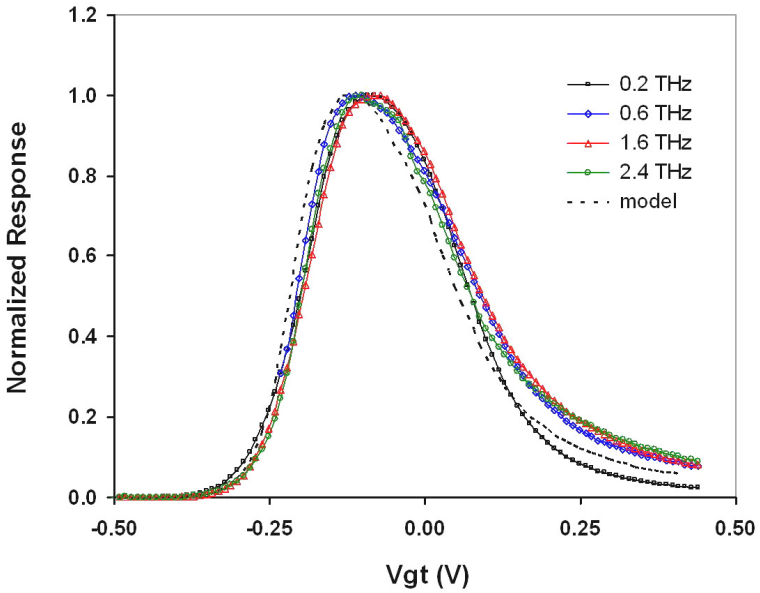

Figure 4 – 20 fin nFET open drain response, normalized to response maxima, across several incident frequencies. $W_f = 40$ nm; $L_g = 100$ nm. Dashed line represents modeled response using eq. (5) with $f = 0.2$ THz.

The response at each frequency is normalized to its peak value to allow direct comparison across the frequency range, and good agreement with the model of eq. (5) is apparent. That the response peaks coincide across the frequency range confirms the non-resonant nature of the response. Figure 5 compares responsivity modeled using eq. (27) to measured data for several FinFET devices. (Calculations of responsivity in measured data are simply measured response divided by incident power; no adjustment for device vs. beam size is used since it is not clear that this approach is warranted [19]). Note that while there are anomalies, the fit is reasonable, especially in the response attenuation at and above 0.6 THz. In addition, note that the FinFET devices in many cases exhibit considerably greater responsivity than standard CMOS FETs.

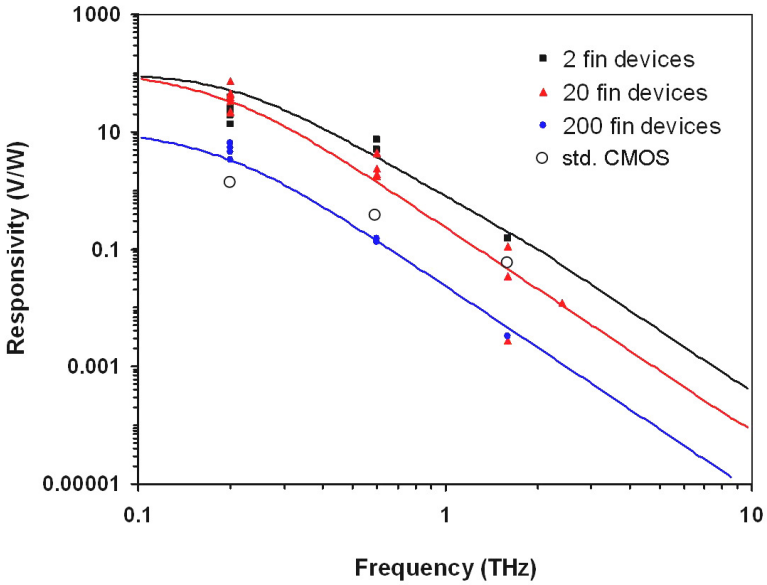

Figure 5 – Open drain responsivity of several FinFET devices at various incident frequencies. Filled symbols are measured data; lines are modeled response using eq. (27) with $L_g = 100$ nm, $L_{pitch} = 200$ nm, $H_f = 40$ nm, $W_f = 60$ nm, $\varepsilon/\delta = 6.9\text{x}10^{-2}$ F/m^2, $\rho_g = 10$ ohms/□, $R_S = R_D = 300$ ohms, $\mu = 0.5$ m^2/Vs, $V_{gt} = -0.1$ V. V_{THz} and L_{THz} were chosen to fit measured data. Open symbols are measured responsivity for standard CMOS FETs. [19, 20]

Responsivity rises dramatically as expected in FinFET devices, reaching from several hundred to above one thousand volts per watt. Figure 6 illustrates the degree to which the enhanced responsivity follows that predicted with eq. (6). In Figure 7 is shown the drain current enhanced responsivity for several FinFETs at various frequencies compared with the response of standard CMOS FET data. Here especially is demonstrated the advantage of the FinFET structure, as responsivity is seen to be nearly two orders of magnitude higher than the standard CMOS FETs.

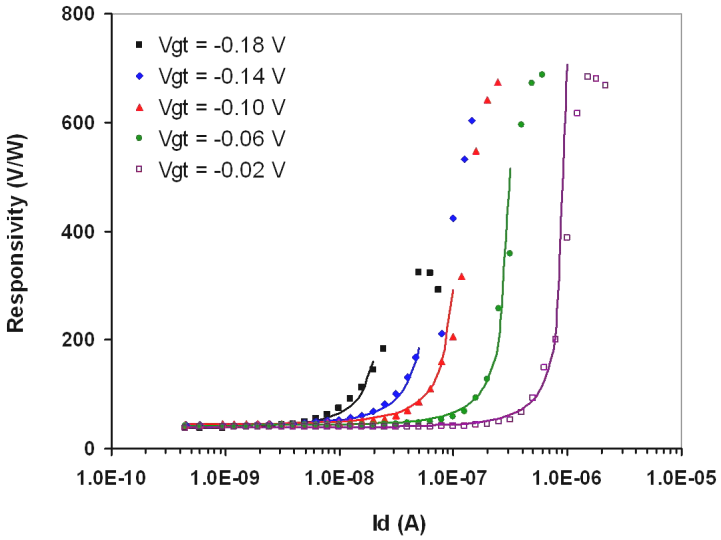

Figure 6 – 0.2 THz responsivity of 20 fin device with $W_f = 40$ nm and $L_g = 100$ nm. Symbols are measured data; lines are modeled responsivity following eq. (6).

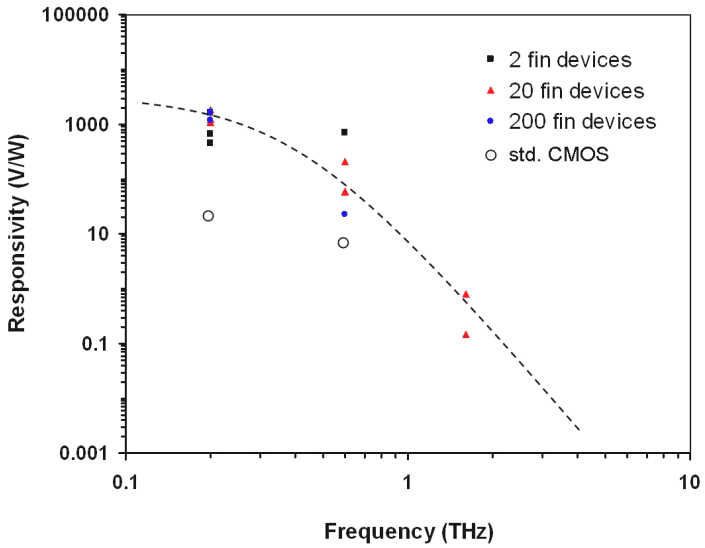

Figure 7 – Peak drain current enhanced responsivity of several FinFET devices vs. incident frequency. Filled symbols are measured data. Dashed line is drawn to guide the eye. Open symbols are measured responsivity for standard CMOS FETs. [20]

5. Noise Equivalent Power

Noise Equivalent Power represents the minimum signal power distinguishable from the detector noise, and is a figure of merit for the detector sensitivity. Commonly, NEP is considered to be the minimum power detectable per square root of bandwidth, in units of W/√Hz, and is calculated as the inverse ratio of responsivity to the square root of device voltage noise. In the open drain configuration, the thermal noise of the channel resistance is predominant [10, 21]. Reducing the channel resistance decreases NEP for a given responsivity by a factor of the square root of the resistance reduction, thus increasing the number of device fins from 2 to 20, or 20 to 200 will decrease the noise contribution to NEP by a factor of ~3.2. Returning to Figure 5 however, finds a decrease in responsivity of one magnitude order between 20 and 200 fin devices, therefore NEP increases for the larger number of fins. This is illustrated in Figure 8.

The comparison between 2 and 20 fins is less clear due to the observed anomalies in responsivity for the 2 fin devices, though in general NEP is expected again to be higher for the larger number of fins.

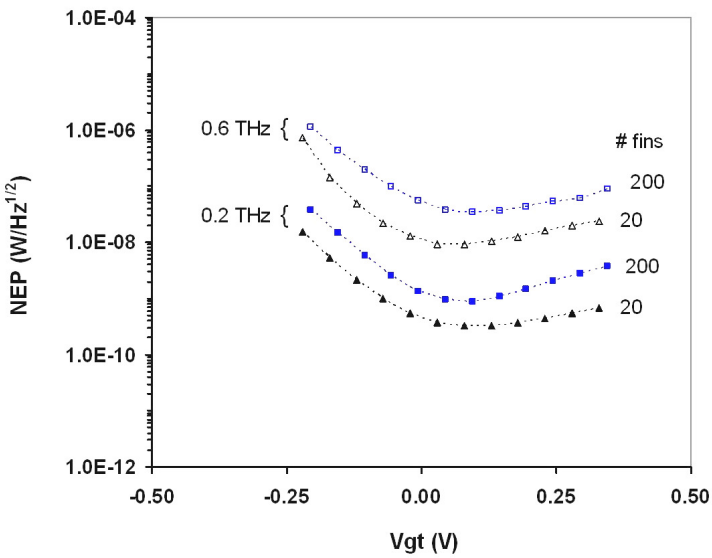

Figure 8 – Noise equivalent power vs. gate bias for two FinFET devices at 0.2 (filled symbols) and 0.6 THz (open symbols) calculated from measured response and channel resistance data. $W_f = 40$ nm, $L_g = 60$ nm, 20 fins (triangles) and 200 fins (squares).

Estimation of NEP becomes more complicated with the introduction of drain current. Responsivity increases on average between 20 and 30 times that of the open drain response for the FinFET devices; however device noise increases dramatically as well, essentially as a function of the drain current squared. The noise spectra are seen to follow

a $1/f^a$ distribution, with $a \approx 1$, as is shown in Figure 9. Here the spectrum measured with a drain load resistance of 2.5 kohms is used to estimate the spectra with loads more typical of those used in responsivity measurements, allowing comparison of NEP with drain current to that of the open drain configuration.

Peak responsivity for the device in Figure 9 was measured to be 1200 V/W; at the optical chopper frequency used in response measurements of 50 Hz and with an amplifier load of approximately 10 Mohm, the voltage noise density is calculated to be 5 x 10^{-8} V^2/Hz, thus the NEP at 50 Hz is approximately 2 x 10^{-7} W/$Hz^{1/2}$. The sampling frequency required to achieve the open drain NEP for this device of 3 x 10^{-3} W/$Hz^{1/2}$ is calculated to be approximately 35 MHz, well below the ~30 GHz maximum response frequency predicted by eq. (29).

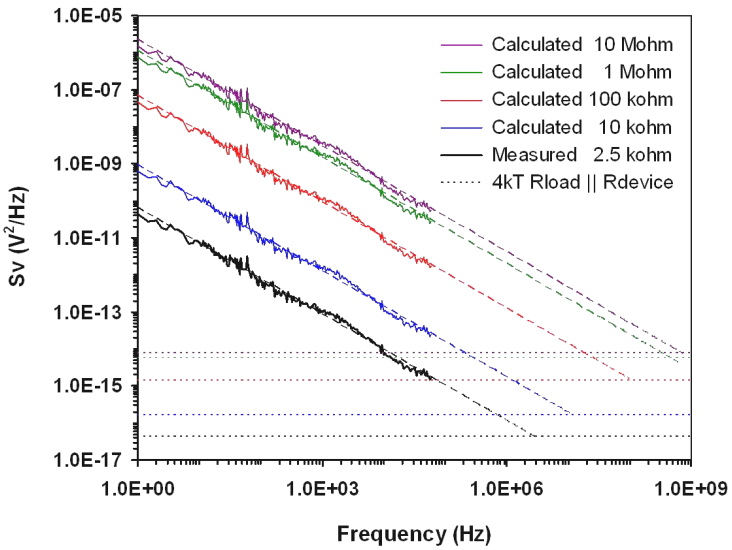

Figure 9 – Voltage noise spectral density for 20 fin device with W_f = 40 nm and L_g = 100 nm. Measured data at V_{gt} = 0V and I_d = 3.1 μA with 2.5 kohm drain load (lowest line) is calculated to show expected device noise for larger values of load resistance (responsivity measurements presented earlier are loaded at 10 Mohm). Horizontal dashed lines are corresponding calculated thermal noise values; angled dashed lines project device noise to these values to indicate frequencies of equivalence.

6. Conclusion

We have demonstrated the response of Si FinFETs to terahertz and sub-terahertz radiation and developed a model to explain the observed decrease in response as the number of device fins increases, which we attribute to the attenuation of the coupled incident radiation both across the device gate conductor transmission line and due to the inductance of the device bond wires. Our results show that narrow FinFETs can be

competitive or better than commercial THz detectors potentially enabling the development of sub-THz and THz cameras implemented using this technology.

Acknowledgments

The work at RPI is supported by SEMATECH, by the InterconnectFocusCenter, and by the NSF under the auspices of the I/UCRC "CONNECTION ONE".

References

[1] W. J. Stillman and M. S. Shur, "Closing the Gap: Plasma Wave Electronic Terahertz Detectors," *Journal of Nanoelectronics and Optoelectronics*, vol. 2, pp. 209-221, 2007.

[2] T. A. Elkhatib, A. V. Muravjov, D. B. Veksler, W. J. Stillman, X.-C. Zhang, M. S. Shur, and V. Y. Kachorovskii, "Subwavelength Detection of Terahertz Radiation using GaAs HEMTs," Proceedings of IEEE Sensors, pp. 1988-1990, 2009.

[3] QMC_Instruments, http://www.terahertz.co.uk/,2010

[4] Spectrum_Detector_Inc., http://www.spectrumdetector.com/pdf/datasheets/THZ.pdf,2007

[5] Virginia_Diodes_Inc,http://virginiadiodes.com/WR2.2ZBD.htm,2007

[6] M. Dyakonov and M. Shur, "Shallow water analogy for a ballistic field effect transistor: New mechanism of plasma wave generation by dc current," *Physical Review Letters*, vol. 71, pp. 2465-2468, 1993.

[7] M. I. Dyakonov and M. S. Shur, "Plasma wave electronics: Novel terahertz devices using two dimensional electron fluid," *IEEE Transactions on Electron Devices*, vol. 43, pp. 1640-1645, 1996.

[8] M. Dyakonov and M. Shur, "Detection, mixing, and frequency multiplication of terahertz radiation by two-dimensional electronic fluid," *IEEE Transactions on Electron Devices*, vol. 43, pp. 380-387, 1996.

[9] W. Knap, V. Kachorovskii, Y. Deng, S. Rumyantsev, J. Q. Lu, R. Gaska, M. S. Shur, G. Simin, X. Hu, M. Asif Khan, C. A. Saylor, and L. C. Brunel, "Nonresonant detection of terahertz radiation in field effect transistors," *Journal of Applied Physics*, vol. 91, pp. 9346, 2002.

[10] W. Stillman, M. S. Shur, D. Veksler, S. Rumyantsev, and F. Guarin, "Device loading effects on nonresonant detection of terahertz radiation by silicon MOSFETs," *Electronics Letters*, vol. 43, pp. 422-423, 2007.

[11] J. Q. Lu and M. S. Shur, "Terahertz detection by high-electron-mobility transistor: Enhancement by drain bias," *Applied Physics Letters*, vol. 78, pp. 2587, 2001.

[12] D. Veksler, F. Teppe, A. P. Dmitriev, V. Y. Kachorovskii, W. Knap, and M. S. Shur, "Detection of terahertz radiation in gated two-dimensional structures governed by dc current," *Physical Review B (Condensed Matter and Materials Physics)*, vol. 73, pp. 125328-1, 2006.

[13] M. Schubert, B. Hofflinger, and R. P. Zingg, "A one-dimensional analytical model for the dual-gate-controlled thin-film SOI MOSFET," *Electron device letters*, vol. 12, pp. 489-491, 1991.

[14] D. J. Frank, S. E. Laux, and M. V. Fischetti, "Monte Carlo simulation of a 30 nm dual-gate MOSFET: how short can Si go?," International Electron Devices Meeting 1992. Technical Digest (Cat. No.92CH3211-0), pp. 553-6, 1992.

[15] K. Suzuki, T. Tanaka, Y. Tosaka, H. Horie, and Y. Arimoto, "Scaling theory for double-gate SOI MOSFET's," *IEEE Transactions on Electron Devices*, vol. 40, pp. 2326-9, 1993.

[16] C. Fiegna, H. Iwai, T. Wada, M. Saito, E. Sangiorgi, and B. Ricco, "Scaling the MOS transistor below 0.1 m: methodology, device structures, and technology requirements," *IEEE Transactions on Electron Devices*, vol. 41, pp. 941-51, 1994.

[17] D. Hisamoto, L. Wen-Chin, J. Kedzierski, H. Takeuchi, K. Asano, C. Kuo, E. Anderson, K. Tsu-Jae, J. Bokor, and H. Chenming, "FinFET-a self-aligned double-gate MOSFET scalable to 20 nm," *IEEE Transactions on Electron Devices*, vol. 47, pp. 2320-5, 2000.

[18] V. Y. Kachorovskii and M. S. Shur, "Field effect transistor as ultrafast detector of modulated terahertz radiation," *Solid State Electronics*, vol. 52, pp. 182-5, 2008.

[19] W. J. Stillman, "Silicon CMOS FETs as terahertz and sub-terahertz detectors," in *Doctoral Thesis*. Troy, NY: RPI, 2008.

[20] W. Stillman, F. Guarin, V. Y. Kachorovskii, N. Pala, S. Rumyantsev, M. S. Shur, and D. Veksler, "Nanometer scale complementary silicon MOSFETs as detectors of terahertz and sub-terahertz radiation," IEEE Sensors 2007 Conference, pp. 934-7, 2007.

[21] R. Tauk, F. Teppe, S. Boubanga, D. Coquillat, W. Knap, Y. M. Meziani, C. Gallon, F. Boeuf, T. Skotnicki, C. Fenouillet-Beranger, D. K. Maude, S. Rumyantsev, and M. S. Shur, "Plasma wave detection of terahertz radiation by silicon field effects transistors: Responsivity and noise equivalent power," *Applied Physics Letters*, vol. 89, pp. 253511, 2006.